International Journal of Engineering

Generation Process and Performance Evaluation of Engineered Microsphere Agarose Adsorbent for Application in Fluidized-bed Systems

R. Mofidian[a,b], A. Barati*[a], M. Jahanshahi[b], M. H. Shahavi[c]

[a] Department of Chemical Engineering, Faculty of Engineering, Arak University, Arak, Iran
[b] Nanotechnology Research Institute, Babol Noshirvani University of Technology, Babol, Iran
[c] Faculty of Engineering Modern Technologies, Amol University of Special Modern Technologies (AUSMT), Amol, Iran

P A P E R   I N F O

A B S T R A C T

In this research, the generation process of engineered microsphere agarose adsorbent has been explained that has surfaces with different active sites to adsorb protein nanoparticles into the fluidized-bed system. Also, excellent selectivity of protein nanoparticles, high adsorption capacity, and fast equilibrium rate through the eco-friendly polymeric adsorbents were vital aims in here. Hence, agarose as a cheap, and abundant natural polymer, with a ferromagnetic condenser, and dye-ligand adsorbents, were employed to generate the engineered microsphere agarose adsorbent. Then, the performance of produced adsorbents was evaluated in the batch and fluidized-bed system. Scanning electron microscopy, atomic force microscopy, and optical microscope were used. Results showed the shape of adsorbents is spherical, with the size distribution range of 50-250 µm, the porosity of around 90%, and the wet density of 2.6 g/mL. Then, to compare the performance of the engineered adsorbents in a fluidized-bed system, the dye ligand was immobilized on the Streamline™. The obtained results were compared at the same conditions. In batch adsorption tests, the results of lactoferrin nanoparticle adsorption were shown higher dynamic binding capacity with engineered microsphere agarose adsorbents. Also, the results demonstrated that more than 75% of the adsorption process occurred in the first half-hour, which is a very suitable time for a fluidized-bed system. Also, adsorption equilibrium data were evaluated with isothermal adsorption models, and Langmuir's model suits the data, and the maximum of adsorption was close to 45.3 mg/mL adsorbent. The fluidized-bed adsorption tests showed that engineered adsorbents gained a sound breakthrough performance at high flow velocity and upper dynamic binding capacity compared to commercial adsorbents. The dynamic binding capacity at 10% breakthrough achieved 71% of the flooded adsorption process at the major fluid velocity of 348 cm/h, so the engineered adsorbent has been proved the good potential for use in high flow rate fluidized-bed systems.

doi: 10.5829/ije.2020.33.08b.02

1. INTRODUCTION

Based on chemical engineering knowledge, one can develop a new multi-functional adsorbents for efficient protein nanoparticle adsorption in fluidized-bed systems. In the generation process of engineered microsphere polymeric adsorbents, excellent selectivity of nanoparticles, high adsorption capacity, and the fast equilibrium rate through economic polymeric substances are vital factors produced in every industrial system [1-3]. Accordingly, the use of natural origin polymeric substances is significant. Agarose is a natural-originated marine polysaccharide polymer having unique characteristics that give reason to consider it for engineering applications. There are several types of agarose available in the chemical market. One of the most important of them is low-melting agarose, which is used in the adsorption process. The agglomeration of agarose increases by adding metal elements such as nickel, zinc, or fill materials such as cellulose bead, silica gel, zirconium oxide, titanium oxide, and stainless steel. Solid filler materials and other porous solids can be used to increase the density of these products [4-6]. A metallic core adsorbent with a porous surface is an ideal choice

for this purpose. Choosing the right metal core results in adsorption with a specific density and excellent performance [7-9]. Nickel is corrosion resistant, highly malleable, and fully recyclable so that it is an excellent choice for strengthening composites. Nickel has high polarizability ($\alpha=6.8$), and low ion radius ($Ni^{2+}=0.69$ Å, $Ni^{3+}=0.62$ Å) compared to other metals; therefore, it is used as an absorbent core [10, 11].

By balancing the surface of an oil-impregnated object with water droplets deposited by adhesion force, oil droplets can be changed from hydrophobic to hydrophilic conditions. This physical phenomenon is defined as a three-phase emulsion. There are four main phases embedded in three-phase emulsion systems: water, oil, nanoparticles, and the substrate [12, 13]. Thus, three possible contact interfaces can form (1) oil/water, (2) water/substrate, and (3) oil/substrate. The ease of emulation depends on a variety of factors: interfacial surface tension, viscosity, chemical composition, the content of low molecular weight, and adsorption of different biological substances from intraocular fluids and tissues (emulsifiers). Studies have shown that all of these can have a role in the emulsification process. The affinity of a substance to emulsify and disperse into droplets over time is also reliant on its viscosity. Silicone oils have a high viscosity (1–5.00 cp), and because of their viscosity and their ability to repel water, they are referred to as oils [14-17].

Fluidized-bed adsorption (FBA) is an efficient technique for direct capture of target proteins from unrefined raw materials, as well as improved productivity and process economy. FBA is an ingenious chromatography technique to integrate illumination, concentration, and initial purification into an independent path [18, 19]. Adsorption has long been a research topic in the area of environmental science and engineering, and there is a large number of scientific and technical papers in this area [20, 21]. Adsorption is the process through which a substance, initially present in one phase, is removed from that phase by accumulation at the interface between that phase and a separate (solid) phase [22, 23]. Two essential properties of each adsorbent are size distribution of the particles and high density to provide a stable fluidized-bed, which also encompasses the hydrodynamic properties of the fluidized-bed and the packed bed. High density is needed for a steady operation at higher flow velocity, and the suitable size distribution contributes significantly to a complete mixture in the column [24-26]. A high compressive adsorbent does not need to be recovered because it can hold more adsorbate per unit weight. An essential way to increase the density of the absorbent structure is to increase the flow intensity and consequently increase the particle size. Many types of supporting matrices for FBA have been developed, and their preparation methods have gradually been commercialized [27].

The agarose-nickel adsorbent was initially developed by Asghari et al. [28]. They formulated the novel adsorbent by using the water-in-oil emulsification method. Desirable adsorbents had a spherical appearance, and suitable size distribution, the appropriate wet density of 1.95 g/mL, and porosity of 91.93% [28]. Also, Rezvani et al. [29] showed a higher adsorption rate and binding capacity compared to that of the Streamline™. They prepared two different agarose-nickel bead size with the sizes (75-150 & 150-300 µm) in the subject of hydrodynamic stability and adsorption properties [29]. Mohsenkhani et al. [30] invented a cost-effective series of support matrix named as k-carrageenan-zink. The new matrix had a wide size distribution of 50–350 µm and a mean diameter of 160–230 µm. They were found that increasing the fluid velocity and viscosity could compromise the FBA stability. However, the high flow velocity is most likely required to achieve high productivity and high viscosity in biological feedstocks [30]. In other work, super porous κ-Carrageenan-nickel adsorbent beads have been fabricated and evaluated using water in oil emulsification and granule leaching methods by Abatari et al. [31]. The results indicated that the particles had normal size distribution with the range of 60–320 µm. As a result of physical properties measurements, a proper wet density at the range of 1.43–2.42 g/mL has resulted in the adsorbent beads [31].

In this research, the engineered microsphere agarose (EMA) adsorbent was generated and presented as an adsorbent that has surfaces with different active sites to adsorb protein nanoparticles on the FBA systems. Scanning electron microscopy (SEM), atomic force microscopy (AFM), and optical microscope (OM) techniques have been employed to measure the formation of protein model, shape, and morphology of EMA adsorbents. Also, commercial Streamline™ adsorbent, which is an agarose-based anion exchanger, was prepared with the same dye ligand in a similar technique. Then, EMA was compared with Streamline™ based on contact time with various initial concentrations value of Lactoferrin (LF) nanoparticles as a protein model, and breakthrough curves with different flow velocity in the fluidized-bed system and obtaining adsorption isotherms parameters are the ultimate aims of this research.

2. MATERIALS & METHOD

2. 1. Materials   Ultrapure low gelling temperature agarose, acetone, and glycerol were purchased from Merck (Germany). Sorbitan monooleate (Span® 80), Silicone oil and nickel powder with a bulk density of 1500-2600 Kg/m³ and an average particle size of 10 µm were supplied by Sigma (MO, USA). Commercial Streamline™ adsorbent was purchased from Amersham

Biosciences (Uppsala, Sweden), and Cibacron Blue 3GA dye ligand was bought from AG Scientific Inc. (CA, USA).

2. 2. Generation Process of EMA Adsorbent

The main generation process setup of EMA adsorbents shown in Figure 1. In this research, a cylindrical double wall jacketed glass reactor (T_1) with a diameter (D) of 0.04 m, height (H) of 0.06 m, and a stainless steel Ruston turbine (d = 0.01 m) was placed in it. A second glass vessel (D = 0.04 m (T_2), H = 0.06 m)) was used for slurry EMA adsorbents preparation.

In this process, 300 mL of silicon oil with a certain amount of Span® 80 was poured into a double-layer glass reactor. The reactor was connected by a pump to a water bath at 85 °C heated for 30 min. On the other side, a certain amount of agarose powder was stimulated for 5 min at 80°C in a vessel. Then, the nickel powder was added, and the mixing process lasted for 10 min. The contents of the second reactor were transferred to the vessel and mixed for 20 min at a uniform rate. The oil phase was cooled to 15 ◦C by replacing the hot water with cold water in the water bath. Subsequently, the oil production and the semi-ready adsorbent beads were centrifuged for about 20 min at around 11000 rpm to dissolve the oil and solid phases. Then, the solid phase was transferred from the centrifuge vials with acetone into a flask and placed on a shaker at 150 rpm for 2 hours at ambient temperature to achieve uniform particles. After that, the beads were washed by distilled water to remove oil droplets well from the adsorbents. Finally, the pellets were screened by metal sieves according to their size fraction.

Finally, chemical cross-linking was used by epichlorohydrin, to maintain the composite structure and mechanical strength of EMA beads. The EMA beads with a volume equal to 1M sodium hydroxide containing 5 g/L sodium borohydride were placed on a shaker for 30 min at 150 rpm. Then, epichlorohydrin (up to 2% v/v) was added to the mixture. After that, at 25°C, the solution
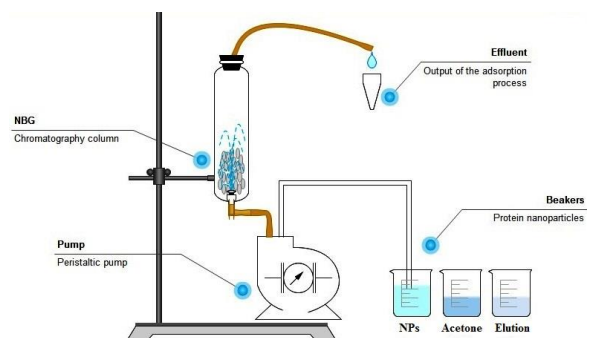
was stirred at 150 rpm for 6 hours on a shaker. Subsequently, the beads were washed with distilled water to separate the ex-reactions. Here, Cibacron Blue 3GA (CB3) was immobilized on the structure of the adsorbent base to prepare EMA adsorbents finally for the processes of adsorption in the fluidized-bed system. The Streamline™'s adsorbent was modified with CB3 by the same method.

2. 3. Adsorption Application

To study the hydrodynamic properties of the EMA adsorbents on the fluidized-bed system, a simple column with an internal diameter of 1 cm and a height of 25 cm was used [32]. A certain amount of adsorbents (around 6 cm bed height) was transferred to the column and allowed to sediment homogeneously. Scheme view of the setup in the fluidized-bed system shown in Figure 2. The adsorbents were washed several times with a 10 mM Tris/HCl buffer at pH 7 to balance its acidity. Then, a certain amount of the adsorbents transferred into the column, and the flow was expanded via the pump. In this study, the acetone solution (10% by volume), and Lf nanoparticles were filled at the floor of the column, and the output effluent of the column was captured in 280 nm wavelength via a spectrophotometer apparatus (Jenway 6305, Germany) [33].

2. 4. Adsorption Characterization

The wet density (ρ_w) was measured by the water replacement method in a test pit and was measured by Equation (1) as below:

$$\rho_p = \frac{M_1 \rho_\omega}{M_1 + M_2 - M_3} \tag{1}$$

where ρ_p and ρ_ω represent the wet density and water density, respectively. M_1, M_2, and M_3 represent the mass of wet adsorbents, the mass of bottle filled with water, and the mass of bottle filled with water and adsorbents. The porosity of the adsorbents was estimated by Equation (2):

Figure 1. The main setup and its various components; (1, 6) Mixtures (2) Reactor T1 (3) Pump (4) Heater (5) Reactor T2 (7) Waterbath

Figure 2. Scheme view of adsorbents application in the FBA systems

$$P = \frac{\omega \rho_p}{\rho_\omega} \times 100\% \tag{2}$$

where ω, is the water content (%) and obtained by Equation (3):

$$\omega = \frac{m_2 - m_3}{m_2 - m_1} \times 100\% \tag{3}$$

where m_1, m_2, and m_3 represent the mass of the weighing bottle, the adsorbent, and weighing bottle before and after drying, respectively [28].

2. 5. Adsorption Isotherms　　　In the kinetic study of adsorption, a batch experiment was carried out using Lf nanoparticles. In summary, 0.9 mL of synthetic adsorbents were poured into a set of 25 mL beakers filled with 10 mL protein of different concentrations as binding for Lf adsorption, and a 1M Tris-HCl buffer stock solution was used. Adsorption trials were perfumed at 20 °C at an incubator speed of 150 rpm to realize the equilibrium. At the end of the process, the protein solution was used to identify protein concentration using a UV detector at a wavelength of 280 nm.

The Langmuir isotherm represents the equilibrium distribution of metal ions between the solid and liquid phases. Based on these assumptions, Langmuir described the following linear Equation (4) [34, 35]:

$$\frac{C_e}{q_e} = \frac{1}{q_m K_L} + \frac{C_e}{q_m} \tag{4}$$

where C_e is equilibrium concentration of adsorbent (mg/mL), q_e is the capacity of adsorption at equilibrium (mg/mL), q_m is the maximum capacity of adsorption (mg/mL) and K_L is the Langmuir isotherm constant. The values of q_m and K_L were calculated based on the slope and intercept of the Langmuir plot of $1/C_e$ versus $1/q_e$.

The Freundlich adsorption isotherm is relative to the adsorption process that occurs on a heterogonous surface. This isotherm provides an expression, which explains the surface heterogeneity. Also, it shows the exponential distribution of active sites and their energies. The linear Equation (5) of the Freundlich isotherm is as follows [36, 37]:

$$\log q_e = \log K_F + \frac{1}{n} \log C_e \tag{5}$$

where K_F and n are the Freundlich isotherm constants that are related to the capacity and intensity of adsorption, respectively. In kinetic reactions, the protein solution is used as a sample to measure the concentration of protein. Equation (6) estimated the sum of adsorbed proteins at each moment [38]:

$$q_t = \frac{C_0 V_0 - C_t V_t}{V_d} \tag{6}$$

where q_t is the volume of dye adsorbed per unit of adsorbent mass (mg/mL), C_0 is initial concentration, and C_t is the concentration of dye (mg/mL) at time t. Moreover, V_0, V_t and V_d are initial volume, the volume of dye solution at time t, and the volume of drained adsorption, respectively.

2. 6. Fluidized Bed Adsorption　　　Dynamic binding capacity (DBC) of a column describes the maximum amount of target protein that can be loaded onto the column without causing unnecessary loss. It is measured under experimental conditions (default flow-rate, real protein sample). As stated above, samples were taken at a specific time interval from the output of the column. The breakthrough curve is obtained by plotting the adsorbed concentration or normalized concentration as a function of the time or flow rate for the given bed height (C/C_0). The shape of this chart may change dramatically in different situations. Here, it is considered as fatigue time when the output concentration reaches 10% of the input concentration ($C/C_0 = 0.1$), and as the time of infiltration ($C/C_0 = 0.9$) when the concentration of output reaches 90%. Since the surface below the infiltration curve represents the amount of protein not absorbed from the column, the dynamic adsorption capacity at the time of infiltration is 10% of the following relationship. This number corresponds to a point in equilibrium temperatures. The following formula measured the DBC of 10% breakthrough curve as Equation (7) [39]:

$$(DBC)q_{10\%} = \frac{C_0 \int_0^{V_{10\%}} (1 - C/C_0) dV}{V_d} \tag{7}$$

where $q_{10\%}$ is the DBC at 10% breakthrough curve and C and C_0 are the outlet and initial concentration of protein, respectively.

2. 7. Preparation of Lf Nanoparticles　　　The Lf nanoparticles were used in the fluidized-bed system to evaluate the new adsorbents. The nanoparticles were prepared in our previous work [40]. Summarily, 3 g Lf powder was poured into 25 mL of distilled water and stirred for 1 hour. Then, the pH of the solution was adjusted to 7. Meanwhile, the Lf solution was heated slowly at a constant rate of 5 °C/min to the final temperature of 90 °C.

3. RESULTS AND DISCUSSION

3. 1. Images Analysis　　　To achieve a microspherical adsorbent is one of the highlights of this work. That as demonstrated in Figure 2a via an optical microscope (Nikon, model YS 100, Japan), the generated EMA particles were to be spherical and micro-sized. As depicted, the particles are defragmented to each other, and all these adsorbent particles have a regular shape. The size range of the EMA adsorbents was 50-250 μm. All adsorbents have physical independence, and there is no adhesion. Schematic of EMA adsorbent drawn in

Figure 2b. As can be seen, nickel particles have shown with black circles that are scattered in the natural agarose polymer. In addition, dye ligands, which are indicated by the blue triangle in Figure 2b, plays an important role due to the mechanism of adsorbent, which acts as a cross-linker between nanoparticles and adsorbents.

Also, the morphology and surface properties of EMA adsorbent were investigated by an SEM (Tescan, Vega XMU-II, Czech Republic) [41]. The acceleration voltage mode of this microscope was changeable between 200 V up to 30 kV, and the resulting magnification could being from 500× up to 3500×. Figures 3a and 3b showed the SEM images of EMA adsorbent. These images can see the porous surface, and the highly reticular structure of adsorbent is evident. Suitable spherical shape and sufficient porosity are of the prominent points in the production of adsorbents. The cavities on the adsorbent are clearly shown in Figure 3b. Also, based on Equation (2), the porosity of particles was measured close to 90%, which is a perfect result for adsorbents.

Lf nanoparticles synthesized and employed in the adsorption process of the fluidized-bed system as a protein model. Morphology and direct physical particle sizes of the Lf nanoparticles determine the AFM images. These images were taken under ambient conditions in the air using an EasySacn II® (NanoSurf Co. Ltd, Liestal, Switzerland). AFM image of Figure 4a shows that the

protein model prepared are in nano-scale and spherical. That indicates that the smaller the particle size, the more surface area is available to the adsorbent, and as a consequence, the higher the number of the binding site available to adsorb it. As can be seen in Figure 4b, the average particle size of Lf nanoparticles in this study was close to 100 nm.

3. 2. Effect of Contact Time It is shown in Figure 5 that for both adsorbents, rapid adsorption of Lf nanoparticle occurred in the very early stages of FBA, which ensured the system equilibrium. As expected, more than 75% of the protein uptake (EMA, 1 mg/mL) occurred during the first half-hour, which is due to soluble droplet inside the column. As can be seen, EMA adsorbents in various concentrations had more adsorption capacity against modified Streamline™ adsorbents. It may be, cause of higher density and porosity of engineered adsorbents. After an hour, the adsorbent function was close to equilibrium for absorbing protein, and the adsorption continued constantly. In a similar study, the same result found that the sorption reached at equilibrium state after 1 hour and revealed an adsorption
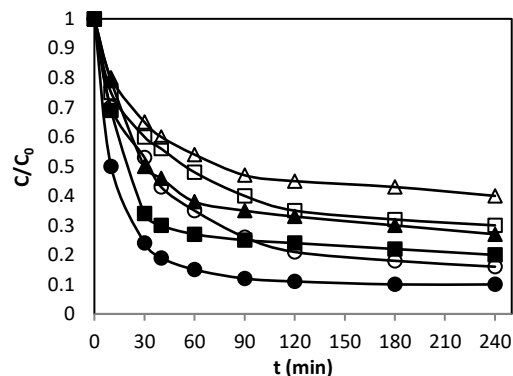

(a)   (b)
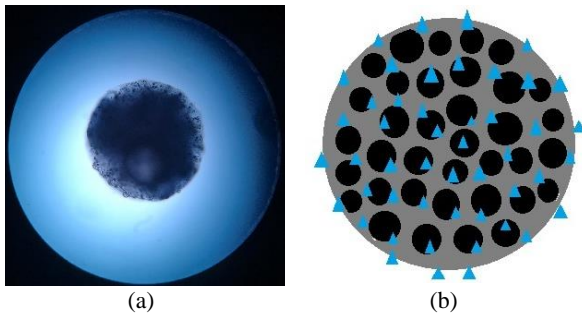
Figure 2. EMA adsorbent (a) optical microscopy image; and (b) schematic image: ▲ dye ligand, ● nickel, ■ agarose

(a)   (b)
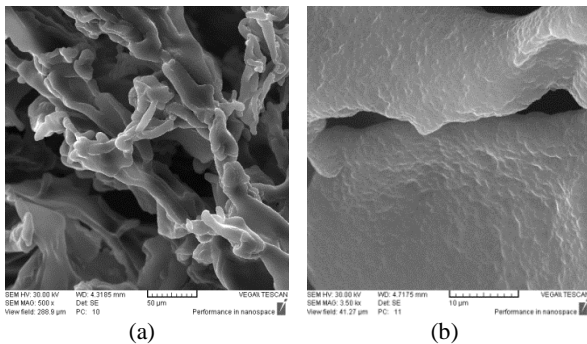
Figure 3. SEM images of a EMA adsorbent (a) 30 kV, magnification 500, (b) 30 kV, magnification 3500


(a)   (b)
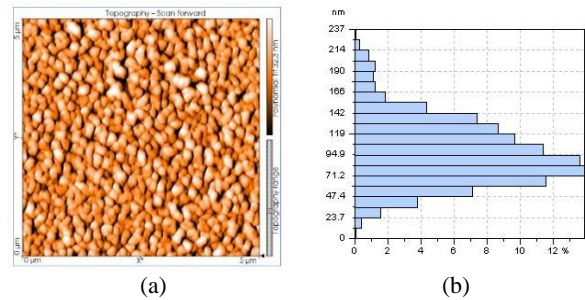
Figure 4. AFM of Lf nanoparticles (a) morphology image, (b) Particle size distribution graph

Figure 5. The Effect of contact time on Lf adsorption against on generated adsorbents with different initial concentrations: (●) EMA, 1 mg/mL; (■) EMA, 2 mg/mL; (▲) EMA, 3 mg/mL; (○) Streamline™, 1 mg/mL; (□) Streamline™, 2 mg/mL; (Δ) Streamline™, 3 mg/mL

efficiency of 98 % [42] whereas, for EMA adsorbents, this occurred after 4 hours, which is due to the presence of porosity that is evident in the synthesized adsorbent. This porosity causes a delay in the equilibrium of the adsorption process, which is a significant factor and increases the adsorptive properties - i.e., DBC [38].

3. 3. Adsorption Isotherms Analyses   The Lf nanoparticles adsorption experimental data obtained from the batch system were used to find the appropriate isotherm model. Freundlich and Langmuir adsorption isotherms were plotted in Figure 6 (q_e versus C_e). According to Equation (4), q_m is related to C_e, q_e, and K_L. Also, from Table 1 could be found the isotherm parameters for the adsorbents by linear regression appear to give acceptable fits to the experimental data with respective regression coefficients (R^2) close to unity. Overall, the Langmuir isotherm has the highest R^2 values, whereas the Freundlich values are considerably lower. The Langmuir monolayer adsorption capacity (q_m) and equilibrium constant (k_L) for Lf nanoparticles adsorbed by EMA are 47 mg/mL and 0.0168 mg/mL, respectively. Also, at the same variables process condition (such as dye-ligand type, contact time, and etc.) the value of the modified Streamline™ adsorption capacity was obtained 43.4 mg/mL. The Langmuir isotherm provide a reasonable description due to the easiness and good agreement with experimental data. Simultaneously, this tentative model supposes monolayer adsorption; in which adsorption can only turn up at a limited number of particular localized sites, which are identical and equivalent, with no costal interaction between the adsorbed molecules, even on adjacent sites [43, 44].
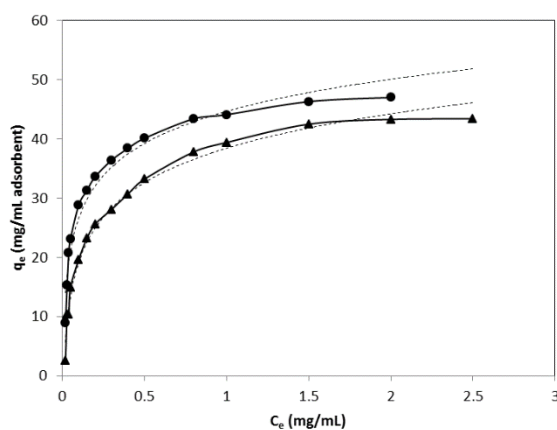
TABLE 1. Parameters of equilibrium isotherms (Langmuir and Freundlich)

Adsorbents	q_{max}	Langmuir model			Freundlich model		
		q_m	K_L	R^2	K_F	n	R^2
EMA	45.3	47	0.0168	0.967	26.4	1.16	0.9443
modified Streamline	40.2	43.4	0.0247	0.977	22.9	1.11	0.9503

3. 4. Breakthrough Curve   The breakthrough curve happens when the concentration of the feed target protein is equal to the concentration of output target protein. It indicates when to stop the loading, depending on how much bed remains unused and lost. Figure 7 shown the breakthrough curve of Lf during binding to EMA and modified Streamline™ adsorbents in the FBA system at the stream rate of 174 cm/h, and a bed height of 6 cm. The results of the breakthrough diagram clearly shown that the adsorption capacity is perfect for the EMA adsorbent ($q_{10\%}$), which can reach more than 90% of the saturated adsorption. This result indicates the size of the small adsorbent beads, which can affect the order of film mass transfer and the mass resistance inside the beads. The sharp breakthrough curve for Streamline™ was obtained even when adsorption was carried out either in highly viscous solutions or at a high velocity of 174 cm/h. However, using frontal analysis, the breakpoint was found to vary in an approximately linear manner with the degree of bed expansion. The breakpoint was also found to occur much earlier when adsorption was carried out at this superficial velocity. This may be the result of either increased mass transfer resistance between Lf in the bulk liquid and adsorption sites in the EMA beads in a high viscosity solution or substantial axial mixing in both the
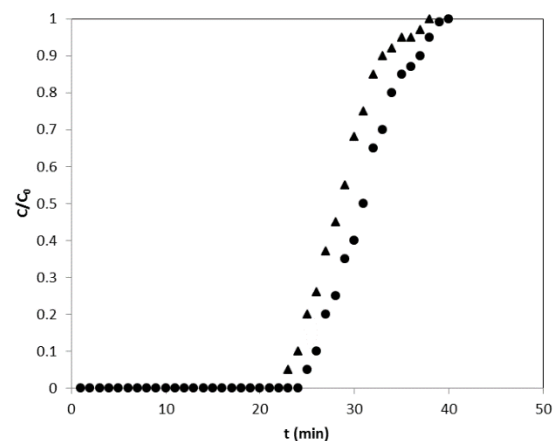

Figure 6. Equilibrium of adsorption isotherms of Lf for (●), EMA; (▲), modified Streamline™; and simulation curves: Langmuir equation (solid lines), Freundlich equation (dashed lines)


Figure 7. Lf nanoparticles breakthrough at the FBA system: (●) EMA, and (▲) modified Streamline™

liquid and solid phases of the adsorbent beds. Similar works have been shown that the shape and position of the breakthrough curves can be affected by the effective diffusivity, external film mass transfer, and solid/liquid phase axial dispersion coefficient.

Moreover, by increasing the flow intensity of 348 cm/h (about 2×) to achieve double bed expansion, the amount of adsorption capacity increased to 10 mg/mL adsorbent, which is very close to the adsorption capacity (9.43 mg/mL adsorbent) for the initial amount of commercial adsorbent (see Figure 8). At this flow rate, the maximum adsorption capacity value is 71%, which is suitable for FBA systems. The results also show that the synthesized EMA adsorbent performs well for high flow rates. As expected, 6 cm bed height is very suitable for commercial adsorption or EMA adsorption to achieve a high DBC.

The EMA adsorbents had an appropriate wet density of 2.6 g/mL. Obviously, the EMA particles with a higher density are suitable for major flow velocity. In comparison with the Streamline™ commercial adsorbents wet density of 1.15 g/mL, novel adsorbents had higher density and an equal range of adsorbents size, which results in less mass transfer resistance and high efficiency for application in fluidized-bed systems.
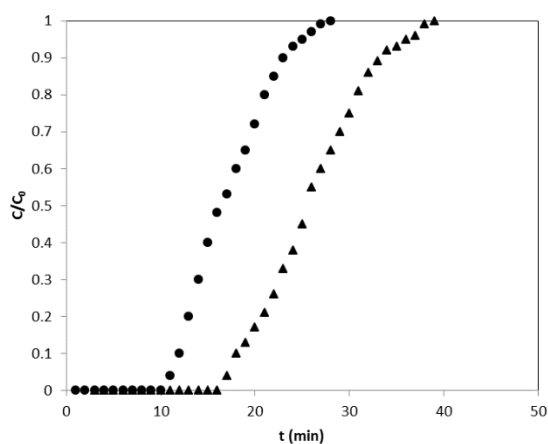
Figure 8. Lf breakthrough curves at 2-fold bed expansion in the FBA system: (●) EMA, and (▲) modified Streamline™

4. CONCLUSION

The preparation of EMA adsorbent was performed using a three-phase emulsion method, and the effects of contact time, adsorption isotherm, DBC, and breakthrough curve on the physical and fluidized bed properties of the beads were investigated. EMA adsorbent immobilized by dye-ligand and showed higher stability in adsorption processes. Suitable porosity, higher density, biodegradability, and ease of operation are the advantages of EMA adsorbent. As mentioned above, the

obtained EMA pellets had an average size of 50-250 µm, a wet density of 2.6 g/mL, and a porosity of 90%. The synthesized adsorbent showed better adsorption efficiency under optimal conditions compared to modified Streamline™ with the same dye-ligand into the FBA system. AFM and OM techniques have been shown the formation of protein model, shape, and morphology of generated EMA adsorbents were to be spherical and micro-sized, respectively. Also, SEM images deliberated that the EMA adsorbents have the porous surface and the highly reticular structure of the adsorbent. Effect of contact time in batch adsorption shows that more than 75% of protein uptake of Lf nanoparticles occurred in the first half of the process that is a good accomplishment since the contact time in FBA systems is not too much. Adsorption isotherms were discussed in this work, and in contrast, the results coincided with the Langmuir model, which indicates that the adsorption was maintained in a single layer. Obviously, in the FBA system, DBC at 10% breakthrough curve and a fluid velocity of 348 cm/h were close to 71%, which helped column efficiency, so the engineered adsorbent has been proved the excellent potential for use in high flow rate fluidized-bed systems.

6. ACKNOWLEDGEMENT

7. REFERENCES

1. Wang, P., Dai, J., Ma, Y., Chen, L. and Pan, J., "Fabrication and evaluation of aminoethyl benzo-12-crown-4 functionalized polymer brushes adsorbents formed by surface-initiated atrp based on macroporous polyhipes and postsynthetic modification", *Chemical Engineering Journal*, Vol. 380, (2020), 122495. https://doi.org/10.1016/j.cej.2019.122495

2. Shahavi, M.H., Hosseini, M., Jahanshahi, M. and Najafpour Darzi, G., "Optimization of encapsulated clove oil particle size with biodegradable shell using design expert methodology", *Pakistan Journal of Biotechnology*, Vol. 12, (2015), 149-160.

3. Arahman, N., Fitri, R.A., Wirakusuma, A., Fahrina, A. and Bilad, M.R., "Adsorption performance of low-cost java plum leaves and guava fruits as natural adsorbents for removal of free fatty acids from coconut oil", *International Journal of Engineering, Transactions A: Basics*, Vol. 32, No. 10, (2019), 1372-1378. doi: 10.5829/ije.2019.32.10a.06.

4. Vesali-Naseh, M., Barati, A. and Vesali Naseh, M.R., "Efficient copper removal from wastewater through montmorillonite-supported hydrogel adsorbent", *Water Environment Research*, Vol. 91, No. 4, (2019), 332-339. doi: 10.1002/wer.1047.

5. Pérez Quiñones, J., Brüggemann, O., Kjems, J., Shahavi, M.H. and Peniche Covas, C., "Novel brassinosteroid-modified polyethylene glycol micelles for controlled release of

agrochemicals", *Journal of Agricultural and Food Chemistry*, Vol. 66, No. 7, (2018), 1612-1619. doi: 10.1021/acs.jafc.7b05019.

6. Mofidian, R., Barati, A., Jahanshahi, M. and Shahavi, M.H., "Fabrication of novel agarose–nickel bilayer composite for purification of protein nanoparticles in expanded bed adsorption column", *Chemical Engineering Research and Design*, Vol. 159, (2020), 291-299. doi: 10.1016/j.cherd.2020.03.024.

7. Mofidian, R., Barati, A., Jahanshahi, M. and Shahavi, M.H., "Agar-zinc adsorbent synthesis with nano cavities to absorb protein nanoparticles", in The 6th International Conference on Composites Characterization, Fabrication and Application (CCFA-6), Iran University of Science and Technology, Tehran, Iran. (2018 of Conference).

8. Hanish, H.H.H., Edrees, S.J. and Shukur, M.M., "The effect of transition metals incorporation on the structural and magnetic properties of magnesium oxide nanoparticles", *International Journal of Engineering, Transactions A: Basics*, Vol. 33, No. 4, (2020), 647-656. doi: 10.5829/ije.2020.33.04a.16.

9. Alizadeh, M., Hosseinzadeh, K., Shahavi, M. and Ganji, D., "Solidification acceleration in a triplex-tube latent heat thermal energy storage system using v-shaped fin and nano-enhanced phase change material", *Applied Thermal Engineering*, Vol. 163, (2019), 114436. doi: 10.1016/j.applthermaleng.2019.114436.

10. Rad, A.S., Samipour, V., Movaghgharnezhad, S., Mirabi, A., Shahavi, M.H. and Moghadas, B.K., "X12n12 (x= al, b) clusters for protection of vitamin c; molecular modeling investigation", *Surfaces and Interfaces*, Vol. 15, (2019), 30-37. doi: /10.1016/j.surfin.2019.02.001.

11. Mashhadzadeh, A.H., Fathalian, M., Ahangari, M.G. and Shahavi, M.H., "Dft study of ni, cu, cd and ag heavy metal atom adsorption onto the surface of the zinc-oxide nanotube and zinc-oxide graphene-like structure", *Materials Chemistry and Physics*, Vol. 220, (2018), 366-373. doi: 10.1016/j.matchemphys.2018.09.016.

12. Shahavi, M.H., Hosseini, M., Jahanshahi, M., Meyer, R.L. and Darzi, G.N., "Evaluation of critical parameters for preparation of stable clove oil nanoemulsion", *Arabian Journal of Chemistry*, Vol. 12, No. 8, (2019), 3225-3230. doi: 10.1016/j.arabjc.2015.08.024.

13. Hosseini, M. and Shahavi, M.H., "Electrostatic enhancement of coalescence of oil droplets (in nanometer scale) in water emulsion", *Chinese Journal of Chemical Engineering*, Vol. 20, No. 4, (2012), 654-658. doi: 10.1016/S1004-9541(11)60231-0.

14. Lashkenari, A.S., Najafi, M., Peyravi, M., Jahanshahi, M., Mosavian, M.T.H., Amiri, A. and Shahavi, M.H., "Direct filtration procedure to attain antibacterial tfc membrane: A facile developing route of membrane surface properties and fouling resistance", *Chemical Engineering Research and Design*, Vol. 149, (2019), 158-168. doi: 10.1016/j.cherd.2019.07.003.

15. Shahavi, M.H., Hosseini, M., Jahanshahi, M., Meyer, R.L. and Darzi, G.N., "Clove oil nanoemulsion as an effective antibacterial agent: Taguchi optimization method", *Desalination and Water Treatment*, Vol. 57, No. 39, (2016), 18379-18390. doi: 10.1080/19443994.2015.1092893.

16. Hosseini, M., Shahavi, M.H. and Yakhkeshi, A., "Ac & dc-currents for separation of nano-particles by external electric field", *Asian Journal of Chemistry*, Vol. 24, No. 1, (2012), 181-184.

17. Kazemeini, H., Azizian, A. and Shahavi, M.H., "Effect of chitosan nano-gel/emulsion containing bunium persicum essential oil and nisin as an edible biodegradable coating on escherichia coli o157:H7 in rainbow trout fillet", *Journal of Water and Environmental Nanotechnology*, Vol. 4, No. 4, (2019), 343-349. doi: 10.22090/jwent.2019.04.008.

18. Driessen, R.T., van der Linden, J.J.Q., Kersten, S.R.A., Bos, M.J. and Brilman, D.W.F., "Characterization of mass transfer in a shallow fluidized bed for adsorption processes: Modeling and supporting experiments", *Chemical Engineering Journal*, Vol. 388, (2020), 123931. doi: 10.1016/j.cej.2019.123931.

19. Shahavi, M., Jahanshahi, M., Najafpour, G., Ebrahimpour, M. and Hosenian, A., "Expanded bed adsorption of biomolecules by nbg contactor: Experimental and mathematical investigation", *World Applied Sciences Journal*, Vol. 13, No. 2, (2011), 181-187.

20. Taheri, E.S., Jahanshahi, M., Hamed Mosavian, M.T. and Shahavi, M.H., "Investigation of hydrodynamic parameters in a novel expanded bed configuration: Local axial dispersion characterization and an empirical correlation study", *Brazilian Journal of Chemical Engineering*, Vol. 29, No. 4, (2012), 725-739. doi: 10.1590/S0104-66322012000400005.

21. Mofidian, R., Shahavi, M.H., Barati, A. and Jahanshahi, M., "Engineering mechanisms for protein nanoparticles adsorption", in The 2th International Conference on Modern Technologies in Sciences, Mazandaran, Iran. (2019 of Conference), 866-871.

22. Asadpour, R., Sapari, N.B., Hasnain Isac, M. and Kakooei, S., "Further study of adsorption of crude oils onto acetylated corn silk and its kinetics and equilibrium isotherm", *International Journal of Engineering, Transactions B: Applications*, Vol. 32, No. 2, (2019), 229-235. doi: 10.5829/ije.2019.32.02b.07.

23. Najafpour, G.D., Shahavi, M.H. and Neshat, S.A., "Assessment of biological hydrogen production processes: A review", *IOP Conference Series: Earth and Environmental Science*, Vol. 36, (2016), 012068. doi: 10.1088/1755-1315/36/1/012068.

24. Askari, M., Salehi, E., Ebrahimi, M. and Barati, A., "Application of breakthrough curve analysis and response surface methodology for optimization of a hybrid separation system consisting of fixed-bed column adsorption and dead-end depth filtration", *Chemical Engineering and Processing-Process Intensification*, Vol. 143, (2019), 107594. doi: 10.1016/j.cep.2019.107594.

25. Shahavi, M.H., Najafpour, G.D. and Jahanshahi, M., "Hydrodynamic behaviour and biochemical characterization of a simple custom expanded bed column for protein purification", *African Journal of Biotechnology*, Vol. 7, No. 23, (2008), 4334-4344.

26. Aminayi, P., Allaedini, G. and Tasirin, S.M., "Hydrodynamic studies of fluidized bed chemical vapor deposition reactors to produce carbon nano tubes via catalytic decomposition over co/pd mgo", *International Journal of Engineering, Transactions C: Aspects*, Vol. 28, No. 12, (2015), 1693-1701. doi: 10.5829/idosi.ije.2015.28.12c.01.

27. Jahanshahi, M. and Shahavi, M.H., Advanced downstream processing in biotechnology, in Biochemical engineering and biotechnology, G. Najafpour Darzi, Editor. 2015, Elsevier. 495-526.

28. Asghari, F., Jahanshahi, M. and Ghoreyshi, A.A., "Preparation and characterization of agarose–nickel nanoporous composite particles customized for liquid expanded bed adsorption", *Journal of Chromatography A*, Vol. 1242, (2012), 35-42. doi: 10.1016/j.chroma.2012.04.019.

29. Rezvani, A., Jahanshahi, M. and Asghari, F., "Characterization of a novel agarose–nickel composite matrix for protein nanoparticles affinity chromatography in expanded bed", *Chromatographia*, Vol. 77, No. 19-20, (2014), 1267-1274. doi: 10.1007/s10337-014-2727-4.

30. Mohsenkhani, S., Jahanshahi, M. and Rahimpour, A., "Cross-linked κ-carrageenan polymer/zinc nanoporous composite matrix for expanded bed application: Fabrication and hydrodynamic characterization", *Journal of Chromatography A*, Vol. 1408, (2015), 178-186. doi: 10.1016/j.chroma.2015.07.018.

31. Abatari, M.N., Emami, M.R.S., Jahanshahi, M. and Shahavi, M.H., "Superporous pellicular κ-carrageenan–nickel composite

beads; morphological, physical and hydrodynamics evaluation for expanded bed adsorption application", *Chemical Engineering Research and Design*,   Vol. 125, (2017), 291-305. doi: 10.1016/j.cherd.2017.07.012.

32. Shahavi, M.H., Najafpour, G. and Jahanshahi, M., "Design and fabrication of expanded bed adsorption column (named nbg-nano bio group) for nanobioproducts separation", **Patent no. IR49023**, 2008, Iran.

33. Shahavi, M.H., Jahanshahi, M., Najafpour, G.D., Ebrahimpour, M. and Hosenian, A.H., "Expanded bed adsorption of biomolecules by nbg contactor: Experimental and mathematical investigation", *World Applied Sciences Journal*, Vol. 13, No. 2, (2011), 181-187.

34. Khavarpour, M., "Adsorption of malachite green from aqueous solution by nanozeolite clinoptilolite: Equilibrium, kinetic and thermodynamic studies", *International Journal of Engineering, Transactions A: Basics*, Vol. 31, No. 1, (2018), 1-11. doi: 10.5829/ije.2018.31.01a.01.

35. Jafari, B., Khatamnejad, H., Shahavi, M.H. and Domeyri Ganji, D., "Simulation of dual fuel combustion of direct injection engine with variable natural gas premixed ratio", *International Journal of Engineering, Transactions C: Aspects*, Vol. 32, No. 9, (2019), 1327-1336. doi: 10.5829/ije.2019.32.09c.14.

36. Alzeyadi, A., Al-Ansari, N., Laue, J. and Alattabi, A., "Study of biomass bottom ash efficiency as phosphate sorbent material", *Civil Engineering Journal*, Vol. 11, No. 5, (2019), 2392-2401. doi: 10.28991/cej-2019-03091419.

37. Jaafar, J., Goh, P.S., Lau, W.J., Shahrin, S. and Fauzi Ismail, A.F., "Adsorptive removal of cr(vi) and cu(ii) ions from water solution using graphene oxide-manganese ferrite (gmf) nanomaterials", *International Journal of Engineering, Transactions B: Applications*, Vol. 31, No. 8, (2018), 1341-1346. doi: 10.5829/ije.2018.31.08b.24.

38. Jahanshahi, M., Najafpour, G., Ebrahimpour, M., Hajizadeh, S. and Shahavi, M.H., "Evaluation of hydrodynamic parameters of fluidized bed adsorption on purification of nano-bioproducts", *physica status solidi c*, Vol. 6, No. 10, (2009), 2199-2206. doi: 10.1002/pssc.200881737.

39. Chu, K.H., "Breakthrough curve analysis by simplistic models of fixed bed adsorption: In defense of the century-old bohart-adams model", *Chemical Engineering Journal*, Vol. 380, (2020), 122513. doi: 10.1016/j.cej.2019.122513.

40. Mofidian, R., Barati, A., Jahanshahi, M. and Shahavi, M.H., "Optimization on thermal treatment synthesis of lactoferrin nanoparticles via taguchi design method", *SN Applied Sciences*, Vol. 1, No. 11, (2019), 1339. doi: 10.1007/s42452-019-1353-z.

41. Theingi, M., Tun, K.T. and Aung, N.N., "Preparation, characterization and optical property of lafeo3 nanoparticles via sol-gel combustion method", *SciMedicine Journal*, Vol. 1, No. 3, (2019), 151-157. doi: 10.28991/SciMedJ-2019-0103-5.

42. Bhatti, Z.A., Qureshi, K., Maitlo, G. and Ahmed, S., "Study of pan fiber and iron ore adsorbents for arsenic removal", *Civil Engineering Journal*, Vol. 6, No. 3, (2020), 548-562. doi: 10.28991/cej-2020-03091491.

43. Palash, M.L., Jahan, I., Rupam, T.H., Harish, S. and Saha, B.B., "Novel technique for improving the water adsorption isotherms of metal-organic frameworks for performance enhancement of adsorption driven chillers", *Inorganica Chimica Acta*, Vol. 501, (2020), 119313. doi: 10.1016/j.ica.2019.119313.

44. Seliem, M.K., Barczak, M., Anastopoulos, I. and Giannakoudakis, D.A., "A novel nanocomposite of activated serpentine mineral decorated with magnetic nanoparticles for rapid and effective adsorption of hazardous cationic dyes: Kinetics and equilibrium studies", *Nanomaterials*, Vol. 10, No. 4, (2020), 684. doi: 10.3390/nano10040684.

Persian Abstract

چکیده

در این تحقیق، فرآیند تولید جاذب میکروکره آگارزی مهندسی شده که دارای سطوح با سایت‌های فعال مختلف جهت جذب نانوذرات پروتئین در سیستم بستر سیال است شرح داده شده است. همچنین ، انتخاب عالی نانوذرات پروتئینی ، ظرفیت جذب بالا و سرعت تعادل سریع از طریق جاذب‌های پلیمری سازگار با محیط زیست از اهداف مهم در اینجا بود. از این رو ، آگارز به عنوان یک پلیمر طبیعی ارزان و فراوان ، با یک ماده چگال فرومغناطیسی به همراه مولکول های رنگی به عنوان عامل جاذب کننده، برای تولید جاذب میکروکره آگارزی مهندسی شده به کار گرفته شد. سپس عملکرد جاذب‌های تولید شده در سیستم ناپیوسته و بستر سیال مورد بررسی قرار گرفت. میکروسکوپ الکترونی روبشی، میکروسکوپ نیروی اتمی و میکروسکوپ نوری مورد استفاده قرارگرفتند. نتایج نشان داد شکل جاذب‌ها کروی هستند و دامنه توزیع آن ۵۰ تا ۲۵۰ میکرومتر ، تخلخل حدود ۹۰٪ و چگالی مرطوب ۲/۶ گرم در میلی لیتر است. سپس، برای مقایسه بهتر عملکرد جاذب‌های مهندسی شده در یک سیستم بستر سیال، لیگاند رنگی بر روی جاذب تجاری استریم لاین تثبیت شد و در شرایط یکسان مورد بررسی و مقایسه قرار گرفت. در جذب ناپیوسته، نتایج جذب نانوذره پروتئینی لاکتوفرین نشان از ظرفیت دینامیکی بالاتر جاذب میکروکره آگارز مهندسی شده داشت. همچنین، نتایج نشان داد که ۷۵٪ فرآیند جذب در نیم ساعت اول اتفاق می افتد که برای جذب نانوذرات پروتئینی در سیستم بستر سیال بسیار مناسب است. همچنین ، داده های تعادل جذب با مدل های جذب ایزوترمال ارزیابی شدند و مدل لانگمیر داده هـــا را بهتر توصیف می نماید و حداکثر جذب نزدیک به ۴۵/۳ میلی گرم در میلی لیتر جاذب بود. تست‌های جذب بستر سیال نشان داد که جاذب‌های مهندسی شده در سرعت جریان بالای خوراک ورودی نیز ظرفیت اتصال دینامیکی بالایی در مقایسه با جاذب های تجاری با سرعت جریان مشابه دارند. همچنین، نتایج بررسی منحنی های رخنه در سرعت جریان بالا ۳۴۸ سانتی متر بر ساعت خوراک ورودی حدود ۷۱ درصد محاسبه شد، بنابراین جاذب مهندسی شده پتانسیل خوبی برای استفاده در سیستم های بستر سیال با سرعت بالا را نشان داده است.